RESEARCH ARTICLES

Disappearance of a massive star in the Andromeda Galaxy due to formation of a black hole

Kishalay De[1,2,3]*, Morgan MacLeod[4], Jacob E. Jencson[5], Elizabeth Lovegrove[6], Andrea Antoni[2], Erin Kara[3], Mansi M. Kasliwal[7], Ryan M. Lau[8], Abraham Loeb[4,9], Megan Masterson[3], Aaron M. Meisner[8], Christos Panagiotou[3], Eliot Quataert[10], Robert Simcoe[3]

When a massive star reaches the end of its lifetime, its core collapses and releases neutrinos that drive a shock into the outer layers (the stellar envelope). A sufficiently strong shock ejects the envelope, producing a supernova. If the shock fails to eject it, the envelope is predicted to fall back onto the collapsing core, producing a stellar-mass black hole (BH) and causing the star to disappear. We report observations of M31-2014-DS1, a hydrogen-depleted supergiant in the Andromeda Galaxy. In 2014, it brightened in the mid-infrared, then from 2017 to 2022, it faded by factors of $\gtrsim 10^4$ in optical light (becoming undetectable) and $\gtrsim 10$ in total light. We interpret these observations, and those of a previous event in NGC 6946, as evidence for failed supernovae forming stellar-mass BHs.

Massive stars [those with initial masses $\gtrsim 10$ solar masses ($M_\odot$)] can expand and become variable toward the end of their lifetime, undergoing luminosity changes that are observable on human timescales (1). These variations can result from unstable nuclear fusion in the core or mass transfer to a binary companion as the star expands (2). Some of these stars end their lives in luminous [$\gtrsim 10^7$ solar luminosities ($L_\odot$)] supernova (SN) explosions, caused by the collapse of the core (3, 4) and subsequent ejection of the stellar envelope by neutrino-powered shocks (1, 5). These core-collapse SNe are routinely observed with optical time-domain surveys (6).

Theoretical models predict that in other massive stars, the neutrino shock fails to eject the envelope, causing most of the stellar material to fall back onto the collapsing core, forming a stellar-mass black hole (BH) (7, 8). Such a star would abruptly disappear after the failed SN (5, 9), although the initial loss of gravitational binding energy (equivalent to ≈ 0.2 to $0.5\ M_\odot$) to neutrino emission (10, 11) and feedback from inefficient accretion (12, 13) are predicted to inject $\sim 10^{45}$ to 10^{49} erg into the stellar envelope. This is sufficient to eject a small fraction of the outer envelope, possibly producing a faint optical transient ($\lesssim 10^6 L_\odot$) (11, 14). A long-lived brightening in mid-infrared (MIR) light can result from the condensation of this material, forming a circumstellar dust shell (15, 16). Observing such low-luminosity stellar eruptions, or stars that disappear without an explosion, requires monitoring individual stars at extragalactic distances (17, 18) with uniform, sensitive searches over years to decades (7).

Observations of a disappearing supergiant

We applied an image subtraction pipeline (19) to the Near-Earth Object Wide-Field Infrared Survey Explorer (NEOWISE) (20) MIR sky survey to search for variable sources in the nearby Andromeda Galaxy and Triangulum Galaxy (also known as M31 and M33, respectively). Using the observations from 2009 to 2022 with 6-month cadence, we searched for luminous MIR transients (21) that would accompany dusty stellar eruptions, such as failed SNe. We identified a faint brightening of a star (hereafter M31-2014-DS1), located in M31 at celestial coordinates of right ascension $00^h45^m13^s.47$, declination $+41°32'33''.14$ (J2000 equinox) (Fig. 1, B to D). Beginning in 2014, this source increased in MIR flux by $\approx 50\%$ over ≈ 2 years, then faded below its initial flux within a year, and continued to fade until 2022 (Figs. 2 and 3 and fig. S1).

We retrieved archival optical light curves of the source from ground- and space-based surveys (21). In optical light, M31-2014-DS1 faded by a factor of $\gtrsim 100$ between 2016 and 2019 and was undetectable in 2023 optical imaging taken by the ground-based MMT Observatory (Fig. 2). This location was also serendipitously imaged by the Hubble Space Telescope (HST) in 2022. We reanalyzed the HST data (21) and found no detection in the optical F606W filter (Fig. 1F) but a faint source ($\gtrsim 10^4 \times$ fainter than the progenitor from 2012) in the near-infrared (NIR) F814W filter (Fig. 1H). We obtained follow-up NIR imaging and spectroscopic observations using the Infrared Telescope Facility and Keck telescopes in 2023 (21), which confirmed a faint red source in the NIR JHK-bands (Figs. 1J and 4B).

This source was previously identified as an irregular variable star (designated V7984 M31B) (22) and classified as a candidate red supergiant (RSG) on the basis of archival NIR colors (23). We used archival HST and Spitzer Space Telescope (SST) observations from 2005 to 2012 (21) to measure the star's spectral energy distribution (SED). We fitted the SED (Fig. 3) with a model of a blackbody photosphere surrounded by a circumstellar dust shell, as expected from mass loss in evolved stars. The best-fitting model (Fig. 3) corresponds to a supergiant star with luminosity $L \approx 10^5\ L_\odot$ and effective temperature $T_{eff} \approx 4500$ K, surrounded by a dust shell with temperature $T_d \approx 870$ K at a radius of ≈ 110 astronomical units (au). Although the star was previously classified as a candidate RSG, this effective temperature is that of a warmer, yellow supergiant (24, 25). The observed red SED is due to reddening by the circumstellar dust, from which we infer a high mass-loss rate of $\approx 10^{-4}\ M_\odot$ year^{-1} (21).

To investigate how these properties varied over time, we applied the same SED model to optical data from the Gaia space telescope and MIR data from NEOWISE (21). The best-fitting models have an almost constant bolometric luminosity (radiated power integrated across all wavelengths) for 1000 days after the MIR brightening began, which then declines by $\gtrsim 10^4 \times$ over the next 1000 days (Fig. 5) (21). During this time, the source became more obscured by dust (Fig. 4 and fig. S5), with the dust shell reaching an optical depth of $\tau \gtrsim 20$ and the central blackbody reducing in radius by a factor of $\gtrsim 5$ (Fig. 4) (21).

Core collapse of a massive star

The abrupt and sustained bolometric fading of M31-2014-DS1 is unlike the variations observed in other massive, evolved stars (26, 27). Some sources exhibit a temporary optical dimming due to episodes of enhanced mass loss and dust formation (28, 29), but this reprocesses the optical emission into the infrared, so the bolometric luminosity remains constant or gets brighter (21) because of ongoing nuclear fusion (and sometimes energy injection from a binary companion) (30, 31). Even with dust obscuration, those sources become brighter in the infrared. Geometric effects such as preferential mass loss along the equator (32) can reduce the fraction of the remnant luminosity that reaches an observer; however, previous calculations have shown that this effect can reduce the observed luminosity by no more than a factor of two (33).

[1]Department of Astronomy and Columbia Astrophysics Laboratory, Columbia University, NY, USA. [2]Center for Computational Astrophysics, Flatiron Institute, NY, USA. [3]Kavli Institute for Astrophysics and Space Research, Massachusetts Institute of Technology, Cambridge, MA, USA. [4]Center for Astrophysics, Harvard University & Smithsonian, Cambridge, MA, USA. [5]IPAC, California Institute of Technology, Pasadena, CA, USA. [6]US Naval Observatory, Washington, DC, USA. [7]Cahill Center for Astrophysics, California Institute of Technology, Pasadena, CA, USA. [8]National Optical-Infrared Astronomy Research Laboratory, National Science Foundation, Tucson, AZ, USA. [9]Black Hole Initiative, Harvard University, Cambridge, MA, USA. [10]Department of Astrophysical Sciences, Princeton University, Princeton, NJ, USA. *Corresponding author. Email: kd3038@columbia.edu
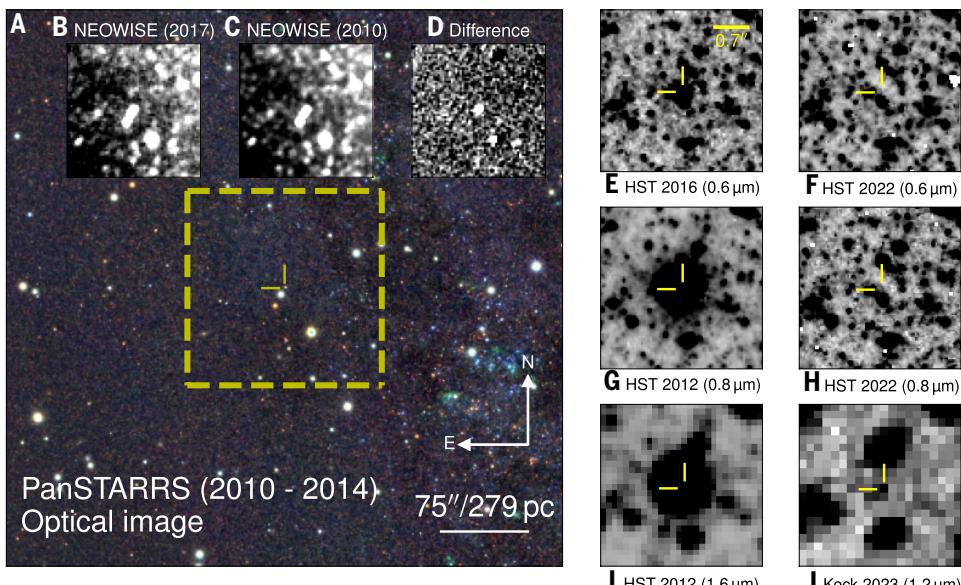
Fig. 1. Location and disappearance of M31-2014-DS1. (**A**) Optical color composite image of the field, taken from the Panoramic Survey Telescope and Rapid Response System (PanSTARRS) PS1 survey (*21*). The yellow dashed square indicates the region shown in (B) to (D), and the yellow cross-hair indicates the position of the star. (**B**) NEOWISE (*20*) MIR image taken in 2017. (**C**) NEOWISE image in 2010. (**D**) The difference between (B) and (C). (**E** to **J**) Zoomed-in images of the star (inverted grayscale) taken in the labeled years: (E) to (H), optical HST images; (I), NIR HST image; and (J), NIR Keck image.

This expectation is consistent with observations of nearby stellar merger remnants with known mass ejection geometry (*33*).

The continuous optical and MIR observations of M31-2014-DS1 during its fading (Fig. 2) show no commensurate increase in infrared brightness, whereas the optical brightness faded by a factor of 10^4. Therefore, the bolometric luminosity reduced. We attribute this to a cessation in nuclear fusion and the collapse of the stellar core. There is no evidence for an associated core-collapse SN, which would have been easily observable. We therefore interpret M31-2014-DS1 as a failed SN in which most of the stellar envelope fell back to form a BH (*7*).

Interpretation as a failed SN

We compare the inferred properties of M31-2014-DS1 to stellar evolution models and the theoretically expected end stages of massive stars. The observed progenitor properties (Fig. 3, between 2005 and 2012) are hotter than predicted for the nominal endpoint of single star evolutionary tracks (*34*), which characterize the progenitors of hydrogen-rich type IIP SNe. However, they are similar to the observed progenitors of some hydrogen-deficient SNe (types IIb and IIL) (*5*). The latter have been interpreted as arising from high mass loss [owing to winds or binary interaction (*35, 36*)] that removed most of the hydrogen-rich stellar envelope. We constructed stellar models of that process (*21*) and found that the closest match with the observed progenitor has a terminal mass of $\approx 5\ M_\odot$, of which $\approx 0.28\ M_\odot$ is the outer hydrogen-rich envelope (Fig. 3B). This model had an initial mass of $\approx 13\ M_\odot$ and is bluer at late times than a hydrogen-rich counterpart without enhanced mass loss (*21*).

We used the optical observations to empirically constrain any mass ejection associated with the collapsing stellar core. On the basis of analytical models for outbursts caused by energy injection into hydrogen-rich envelopes (*37*), we set an upper limit of $\lesssim 0.1\ M_\odot$ ejected material at the star's escape velocity $v_{esc} \approx 60$ km s^{-1}, and corresponding limits of $\lesssim 0.3\ M_\odot$ at $5v_{esc}$ and $\lesssim 1.5\ M_\odot$ at $25v_{esc}$ (Fig. 5A). These constraints imply that most of the $\approx 5\ M_\odot$ star collapsed instead of being ejected, exceeding the maximum mass of a neutron star (*38*) and therefore forming a BH.

If the star were collapsing purely because of its self-gravity, the outer envelope would collapse into the BH within roughly its free-fall time of $t_{ff} \approx \frac{1}{\sqrt{G\rho}} \approx 210$ days, where G is the gravitational constant and ρ is the average stellar density. This is

Fig. 2. Brightness of M31-2014-DS1 as a function of time. The measured flux in millijanskys (left axis) and equivalent luminosity at the distance of the Andromeda Galaxy (right axis), both on logarithmic scales. These are plotted as a function of time in modified Julian date (MJD; bottom axis) and Gregorian year (top axis). Archival data are from the Palomar Transient Factory (PTF), NEOWISE, PS1, Gaia, and the Zwicky Transient Facility (ZTF) surveys; also shown are follow-up photometric data from the MMT Observatory (*21*). Error bars indicate 1σ confidence (smaller than the symbol size for the NEOWISE and pre-2014 data); open symbols with downward arrows indicate 5σ upper limits. For the Gaia photometry, we indicate the raw measurements with light symbols, and the dark symbols indicate the averages within 45 days of the closest epoch of NEOWISE data. The luminosity is expressed as monochromatic λF_λ, where λ is the wavelength and F_λ is the flux density, scaled to a wavelength of 2 μm. In fig. S1, we show the MIR data on an alternative linear scale. All photometric data are provided in our Zenodo data repository (*58*), with references in the supplementary materials (*21*).

Fig. 3. SED and physical properties of the progenitor. (**A**) The ultraviolet to MIR SED of M31-2014-DS1 (solid circles, expressed as monochromatic luminosity λL_λ, where L_λ is the luminosity density) observed with HST and SST from 2005 to 2012. Lines indicate the best-fitting model (parameters are listed in table S2), showing the model's total flux (black solid line), dust emission (orange dot-dashed line), dust-scattered stellar emission (red dashed line), and dust-attenuated stellar emission (blue dotted line). Error bars indicate 1σ confidence (smaller than the symbol sizes), and downward arrows indicate 5σ upper limits. (**B**) The observed luminosity and effective temperature of M31-2014-DS1 (dark green star) compared with theoretical single star evolutionary tracks at different initial masses (colored dashed lines) (*34*). Also shown are the observed progenitor of NGC 6946-BH1 (brown plus symbol) and those of known hydrogen-rich SNe (types indicated in the legend) (*8*). Error bars indicate 1σ confidence. Colored dots are our stellar evolution model for the progenitor of M31-2014-DS1 (*21*), with the residual hydrogen envelope mass indicated by the color bar. The model at the time of core collapse is indicated for M31-2014-DS1 (blue star) and for NGC 6946-BH1 (red plus symbol).
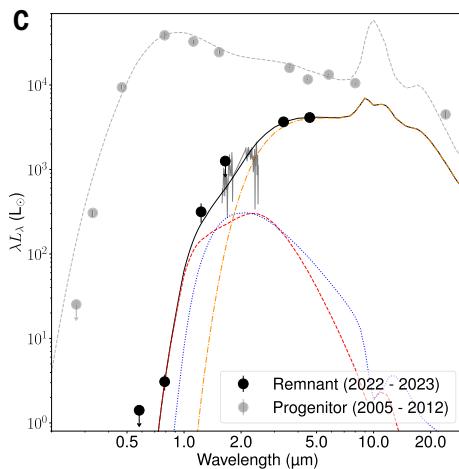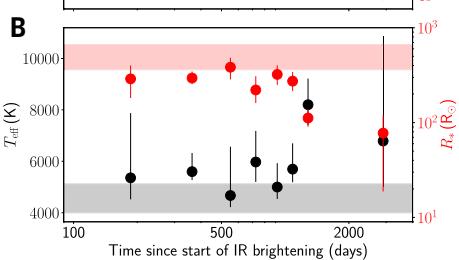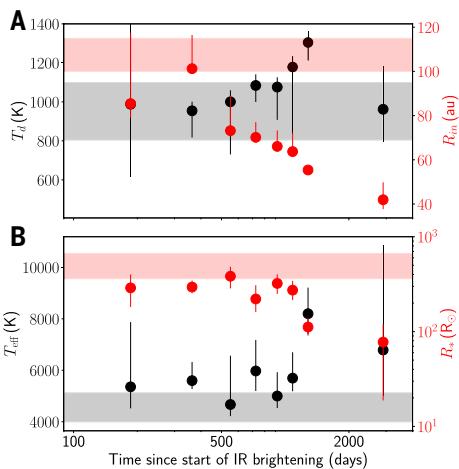
Fig. 4. Evolution of the stellar and dust properties of M31-2014-DS1. Temporal evolution of the dust shell and stellar photosphere inferred from the SED model fitting. (**A**) The dust temperature (T_d; black, left axis) and inner shell radius (R_{in}; red, right axis). (**B**) The effective temperature (T_{eff}; black, left axis) and inferred stellar radius (R_*; red, right axis). (A) and (B) are plotted as functions of time since the start of the MIR brightening in 2014 (on MJD 56674.19) (Fig. 2) (*21*). The shaded regions are the corresponding model parameters for the progenitor from 2005 to 2012. Other parameters are shown in fig. S5. (**C**) The SED of the remnant of M31-2014-DS1 in 2022 to 2023 [photometry in black circles and spectrum in gray lines (shown on a linear scale in fig. S2)]. The best-fitting model is overlain, with line styles as in Fig. 3, and parameters listed in table S2. The corresponding progenitor photometry (gray circles) and SED model (dashed gray line) are shown. Error bars indicate 1σ confidence, and downward arrows indicate 5σ upper limits.

shorter than the observed continued bolometric fading over $\gtrsim 1000$ days (Fig. 5), indicating that the fallback is delayed by energy injected into the outer envelope. To simulate the resulting mass accretion onto the central BH, we took the same hydrogen-depleted progenitor star model as above then added a range of potential shock energies ($\sim 10^{45}$ to 10^{49} erg) injected into the outer envelope. Such shocks are expected from neutrino mass loss and feedback from inefficient accretion (*39–41*) during the collapse of the core. In the final stages of stellar evolution, these outer layers undergo vigorous turbulent convection, which carries substantial angular momentum (*12, 13*) and suppresses direct accretion (*42*). Numerical simulations (*41*) show that $\lesssim 1\%$ of material falling from the outer supergiant envelope accretes directly onto the BH. We adopted an analytic model of the accreted fraction as a function of the relative angular momenta of the fallback material and of an orbit at the BH horizon (*21*).

The resulting models indicate that the mass accretion rate declines rapidly at early times, initially far exceeding the Eddington accretion rate [the maximum accretion rate for which photons can freely escape from near the BH (*43*)]. During this phase, the emergent luminosity is expected (*44*) to be capped near the Eddington luminosity (L_{Edd}), which for a 5 $M_\odot$ BH is $L_{Edd} \approx 6 \times 10^{38}$ erg s^{-1}. This corresponds to material accreting at the Eddington accretion rate, which generates accretion luminosity so that the outward radiation pressure balances the inward gravitational pull of the BH.

Comparing these models to the observations (Fig. 5) indicates that the ≈ 1000-day luminosity plateau can be explained by a super-Eddington accretion phase, during which the emergent source luminosity remains steady at ≈ 30 to 50% L_{Edd}, despite more rapid mass infall. As the infall rate falls below the Eddington rate, the model emergent luminosity becomes proportional to the decaying accretion rate, which is consistent with our observations. Models with higher shock energies unbind a larger fraction of the progenitor envelope, leaving behind a smaller mass that falls back over a shorter period of time. Although we cannot precisely constrain the time of collapse, the fading by a factor of ≈ 10 over ≈ 1000 days is most consistent with shock energies of 10^{47} to 10^{48} erg (Fig. 5). In those cases, $\approx 98\%$ of the stellar mass collapses or falls back, leaving a ≈ 5 $M_\odot$ BH.

Those are weak shock energies compared with that of typical core-collapse SNe ($\sim 10^{51}$ erg) (*5*). They are sufficient to
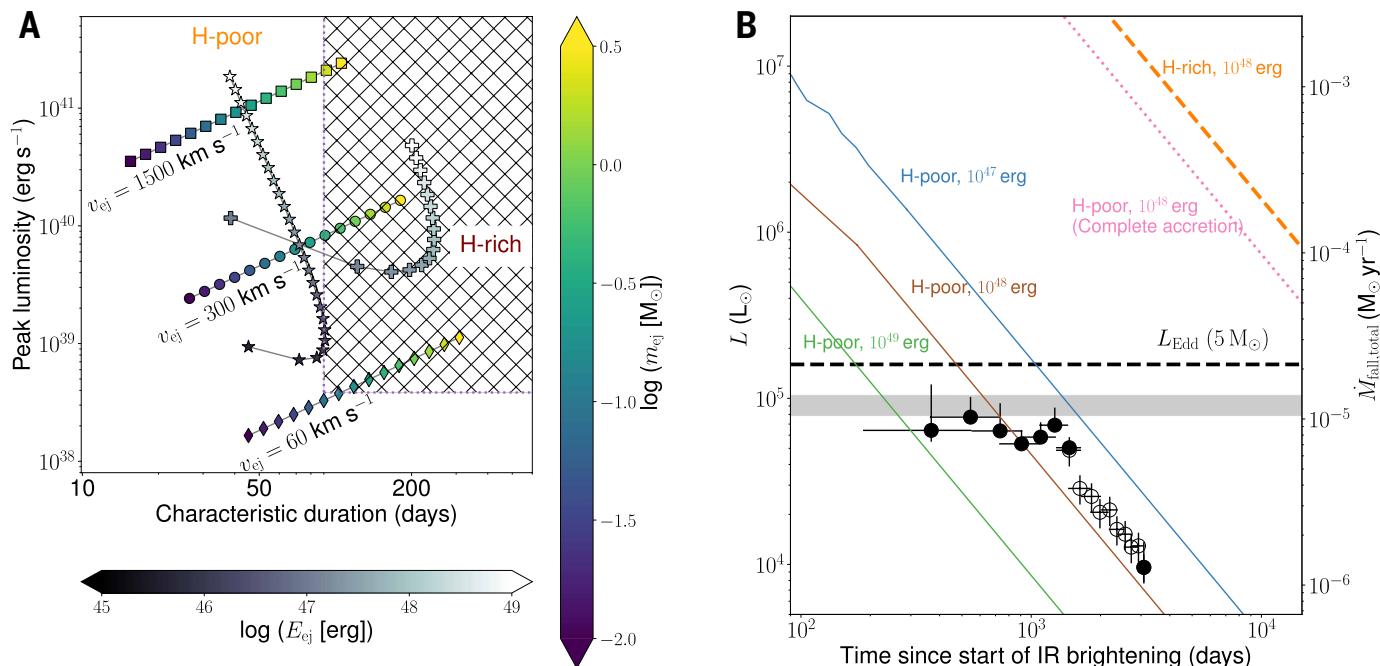
Fig. 5. Constraints on the mass ejection and stellar envelope fallback in M31-2014-DS1. (**A**) The luminosity and duration of transients powered by energy injection into hydrogen-rich envelopes, for ejecta with different velocities (v_{ej}) and kinetic energies (E_{ej}). The diamonds, circles, and squares indicate ejecta with velocities of $\approx 1\times$, $\approx 5\times$, and $\approx 25\times$ the progenitor's escape velocity, respectively, with colors indicating ejecta mass (m_{ej}; right color bar). The cross-hatched area indicates the phase space ruled out by the optical photometry (*21*). Also shown are the luminosity and transient duration for the hydrogen-poor (star symbols) and hydrogen-rich (plus symbols) models as a function of ejecta kinetic energy (bottom color bar). (**B**) The bolometric fading of M31-2014-DS1 (data points) compared with models of mass fallback rates for different explosion energies (green, brown, and blue lines, as labeled). These models assume 5% accretion radiative efficiency. For comparison, we also show 100% accretion (pink dotted line) and an example hydrogen-rich case (orange dashed line). Black solid circles indicate parameters inferred from the SED models, and hollow circles indicate estimates by using a bolometric correction to MIR luminosity (*21*). Error bars indicate 1σ confidence. The gray shaded region indicates the progenitor luminosity, and the black dashed line indicates the Eddington luminosity (L_{Edd}) for a 5 $M_\odot$ BH. The right axis defines the corresponding total mass fallback rate ($\dot{M}_{fall,total}$) from the models.

unbind $\lesssim 0.1\,M_\odot$ of the outer envelope, which would produce a luminous optical outburst that is sufficiently brief to have been missed by observations, given the photometric cadence (Fig. 5). We expect the ejected mass to carry a distribution of velocities as it moves outward and cools (*21*). Most of the material would reach the dust condensation radius (r_c), at which solid dust grains begin to condense from the ejecta. This would produce hot dust on a timescale of $\sim r_c/v_{esc} \approx 30$ au/ 60 km s$^{-1} \approx 900$ days after the ejection, which is consistent with the time of the observed peak MIR flux. Although the details of the dust formation are sensitive to the velocity distribution and dust formation process (*30*), our model velocity distributions (*21*) imply that the fraction of the total ejecta in the hot dust shell (near r_c) is $f_{shell} \approx 0.1$ at any given time. The hot dust mass in the shell is therefore $m_{shell} \sim f_{shell} M_g r_{dg}$, where M_g is the total ejected gas mass ($\sim 0.1\,M_\odot$) and $r_{dg} \approx 0.01$ (*45, 46*) is the assumed dust-to-gas mass ratio. We found that $m_{shell} \sim 10^{-4}\,M_\odot$, which is similar to the dust mass derived from the SED ($\approx 1.1 \times 10^{-4}\,M_\odot$) (fig. S5).

Unified model for a previous candidate

A candidate disappearing supergiant (designated NGC 6946-BH1) has previously been identified in the galaxy NGC 6946 (*16, 47, 48*). In Fig. 3, we also show its progenitor, for comparison with M31-2014-DS1. NGC 6946-BH1 exhibited a luminous ($\sim 10^{-6}\,L_\odot$) optical outburst, followed by an expanding dusty envelope, implying ~ 0.1 to $1\,M_\odot$ of ejecta (*48*). This was consistent with predictions of either failed SNe from hydrogen-rich progenitors (*11*) or some types of stellar mergers (*32, 49*). The dust-obscured remnant then faded to $\approx 15\%$ ($\sim 10^{38}$ erg

s^{-1}) of the progenitor luminosity in ≈ 3000 days (*16*), indicating the termination of nuclear fusion (*50*). However, this is difficult to reconcile with the decades-long ($\gtrsim 10^5$ days) super-Eddington phase for massive hydrogen-rich stars (*48, 51*), during which the emergent luminosity is expected to be constant near the BH Eddington limit ($\sim 10^{39}$ erg s^{-1}). By constructing a hydrogen-rich RSG progenitor model (*21*) that matches the M31-2014-DS1 progenitor luminosity, we confirmed that rapid fading timescales of a few years cannot be explained with stars that have largely retained their hydrogen-rich envelopes (Fig. 5).

The progenitor of NGC 6946-BH1 was initially identified as an RSG (*16, 47*). Later analysis found that it was hotter than expected for single-star RSG evolution (Fig. 3), being more consistent with a yellow supergiant (*52*). We compared its properties with our models and found that the closest match is a progenitor with an initial mass of 17.5 $M_\odot$ with enhanced late-stage mass loss, which forms a hydrogen-depleted star with a terminal mass of $\approx 7.5\,M_\odot$, of which $\approx 0.6\,M_\odot$ is the hydrogen-rich envelope (Fig. 3) (*21*). Applying a similar analysis as for M31-2014-DS1 (*21*), we calculated that the NGC 6946-BH1 model's hydrogen-rich envelope, which is twice as massive, produces an outburst of longerduration (~ 150 days), as observed. Our calculated accretion-powered plateau and fallback timescale (~ 3000 d) are consistent with the bolometric fading of NGC 6946-BH1 (*21, 49, 50*).

M31-2014-DS1 has more archival data available than does NGC 6946-BH1, which excludes a similar optical outburst and better constrains the fading timescale, which we connect with our hydrogen-depleted progenitor model. Nevertheless, the similarities between

M31-2014-DS1 and NGC 6946-BH1 lead us to conclude that they were both associated with the core collapse of massive hydrogen-depleted stars that produced stellar-mass BHs. Accretion onto the BHs might produce x-ray emission, but that has not been detected for either M31-2014-DS1 [from archival x-ray observations (21)] or NGC 6946-BH1, which is explained by x-ray absorption by the surrounding gas (21, 48, 53). Theoretical models of BH formation from massive stars predict a wide range of stellar progenitors (54, 55), with few observational constraints. Using previous estimates for the fraction of failed SNe (18, 56, 57), we calculated that the probability of us identifying at least one event in our search is 1 to 20% (21). Our calculated stellar evolution of M31-2014-DS1 is similar to that of many core collapse SN progenitors (Fig. 3), implying a complex (possibly chaotic) relationship between stellar birth mass and BH formation for stars with initial masses $\gtrsim 12\,M_\odot$, as previously predicted on theoretical grounds (54, 55).

REFERENCES AND NOTES

1. N. Langer, *Annu. Rev. Astron. Astrophys.* **50**, 107–164 (2012).
2. N. Smith, W. Li, J. M. Silverman, M. Ganeshalingam, A. V. Filippenko, *Mon. Not. R. Astron. Soc.* **415**, 773–810 (2011).
3. H. T. Janka, K. Langanke, A. Marek, G. Martínez-Pinedo, *Phys. Rep.* **442**, 38–74 (2007).
4. A. Burrows, D. Vartanyan, *Nature* **589**, 29–39 (2021).
5. S. J. Smartt, *Annu. Rev. Astron. Astrophys.* **47**, 63–106 (2009).
6. D. A. Perley *et al.*, *Astrophys. J.* **904**, 35 (2020).
7. C. S. Kochanek *et al.*, *Astrophys. J.* **684**, 1336–1342 (2008).
8. S. J. Smartt, *Publ. Astron. Soc. Aust.* **32**, e016 (2015).
9. E. O'Connor, C. D. Ott, *Astrophys. J.* **730**, 70 (2011).
10. D. K. Nadyozhin, *Astrophys. Space Sci.* **69**, 115–125 (1980).
11. E. Lovegrove, S. E. Woosley, *Astrophys. J.* **769**, 109 (2013).
12. A. Gilkis, N. Soker, *Astrophys. J.* **827**, 40 (2016).
13. E. Quataert, D. Lecoanet, E. R. Coughlin, *Mon. Not. R. Astron. Soc.* **485**, L83–L88 (2019).
14. E. Lovegrove, S. E. Woosley, W. Zhang, *Astrophys. J.* **845**, 103 (2017).
15. C. S. Kochanek, *Mon. Not. R. Astron. Soc.* **444**, 2043–2047 (2014).
16. S. M. Adams, C. S. Kochanek, J. R. Gerke, K. Z. Stanek, X. Dai, *Mon. Not. R. Astron. Soc.* **468**, 4968–4981 (2017).
17. T. M. Reynolds, M. Fraser, G. Gilmore, *Mon. Not. R. Astron. Soc.* **453**, 2886–2900 (2015).
18. J. M. M. Neustadt *et al.*, *Mon. Not. R. Astron. Soc.* **508**, 516–528 (2021).
19. K. De *et al.*, *Nature* **617**, 55–60 (2023).
20. A. Mainzer *et al.*, *Astrophys. J.* **792**, 30 (2014).
21. Materials and methods are available as supplementary materials.
22. J. Kaluzny *et al.*, *Astron. J.* **115**, 1016–1044 (1998).
23. P. Massey, K. F. Neugent, E. M. Levesque, M. R. Drout, S. Courteau, *Astron. J.* **161**, 79 (2021).
24. E. R. Beasor, N. Smith, J. E. Andrews, *Astrophys. J.* **952**, 113 (2023).
25. R. M. Humphreys, T. J. Jones, J. C. Martin, *Astron. J.* **166**, 50 (2023).
26. C. Conroy *et al.*, *Astrophys. J.* **864**, 111 (2018).
27. M. D. Soraisam *et al.*, *Astrophys. J.* **893**, 11 (2020).
28. J. E. Jencson *et al.*, *Astrophys. J.* **930**, 81 (2022).
29. A. K. Dupree *et al.*, *Astrophys. J.* **936**, 18 (2022).
30. C. S. Kochanek, *Astrophys. J.* **743**, 73 (2011).
31. N. Smith, D. J. Frew, *Mon. Not. R. Astron. Soc.* **415**, 2009–2019 (2011).
32. A. Kashi, N. Soker, *Mon. Not. R. Astron. Soc.* **467**, 3299–3305 (2017).
33. C. S. Kochanek, *Mon. Not. R. Astron. Soc.* **529**, 1958–1969 (2024).
34. J. Choi *et al.*, *Astrophys. J.* **823**, 102 (2016).
35. C. Georgy, *Astron. Astrophys.* **538**, L8 (2012).
36. S.-C. Yoon, M. Cantiello, *Astrophys. J. Lett.* **717**, L62–L65 (2010).
37. D. Kasen, S. E. Woosley, *Astrophys. J.* **703**, 2205–2216 (2009).
38. V. Kalogera, G. Baym, *Astrophys. J.* **470**, L61–L64 (1996).
39. E. Quataert, D. Kasen, *Mon. Not. R. Astron. Soc.* **419**, L1–L5 (2012).
40. M. Ivanov, R. Fernández, *Astrophys. J.* **911**, 6 (2021).
41. A. Antoni, E. Quataert, *Mon. Not. R. Astron. Soc.* **525**, 1229–1245 (2023).
42. J. M. Blondin, *Astrophys. J.* **308**, 755 (1986).
43. Y.-F. Jiang, L. Dai, Numerical simulations of super-eddington accretion flows. arXiv:2408.16856 [astro-ph.HE] (2024).
44. Y.-F. Jiang, J. M. Stone, S. W. Davis, *Astrophys. J.* **796**, 106 (2014).
45. V. Karambelkar *et al.*, Hot springs and dust reservoirs: JWST reveals the dusty, molecular aftermath of extragalactic stellar mergers. arXiv:2508.03932 [astro-ph.SR] (2025).
46. T. Kamiński *et al.*, *Astron. Astrophys.* **655**, A32 (2021).
47. J. R. Gerke, C. S. Kochanek, K. Z. Stanek, *Mon. Not. R. Astron. Soc.* **450**, 3289–3305 (2015).
48. C. M. Basinger, C. S. Kochanek, S. M. Adams, X. Dai, K. Z. Stanek, *Mon. Not. R. Astron. Soc.* **508**, 1156–1164 (2021).
49. E. R. Beasor *et al.*, *Astrophys. J.* **964**, 171 (2024).
50. C. S. Kochanek, J. M. M. Neustadt, K. Z. Stanek, *Astrophys. J.* **962**, 145 (2024).
51. R. Fernández, E. Quataert, K. Kashiyama, E. R. Coughlin, *Mon. Not. R. Astron. Soc.* **476**, 2366–2383 (2018).
52. R. M. Humphreys, *Res. Notes AAS* **3**, 164 (2019).
53. S. Balberg, L. Zampieri, S. L. Shapiro, *Astrophys. J.* **541**, 860–882 (2000).
54. T. Sukhbold, T. Ertl, S. E. Woosley, J. M. Brown, H. T. Janka, *Astrophys. J.* **821**, 38 (2016).
55. L. Boccioli, L. Roberti, *Universe* **10**, 148 (2024).
56. S. M. Adams, C. S. Kochanek, J. R. Gerke, K. Z. Stanek, *Mon. Not. R. Astron. Soc.* **469**, 1445–1455 (2017).
57. R. A. Byrne, M. Fraser, *Mon. Not. R. Astron. Soc.* **514**, 1188–1205 (2022).
58. K. De, M. MacLeod, dekishalay/M31-2014-DS1: Release of MMT data. Zenodo (2025); https://doi.org/10.5281/zenodo.17774115.

Disappearance of a massive star in the Andromeda Galaxy due to formation of a black hole

Kishalay De, Morgan MacLeod, Jacob E. Jencson, Elizabeth Lovegrove, Andrea Antoni, Erin Kara, Mansi M. Kasliwal, Ryan M. Lau, Abraham Loeb, Megan Masterson, Aaron M. Meisner, Christos Panagiotou, Eliot Quataert, and Robert Simcoe

Editor's summary

In a dying massive star, the core collapses to form a compact object. Simultaneously, the outer layers can be ejected at high speed, which is observed as a supernova. Theory predicts that sometimes the ejection speed is too low to escape the gravitational field, so the outer layers fall back over several years, producing no supernova and a more massive compact object. De *et al.* have identified a supergiant star in the nearby Andromeda Galaxy that brightened in the infrared then decreased in optical brightness over the next few years until it became undetectable. They attribute this behavior to a failed supernova and the formation of a black hole. —Keith T. Smith

View the article online
https://www.science.org/doi/10.1126/science.adt4853
Permissions
https://www.science.org/help/reprints-and-permissions

Use of this article is subject to the Terms of service